Eur. Phys. J. Plus (2017) **132**: 7
DOI 10.1140/epjp/i2017-11287-1

THE EUROPEAN PHYSICAL JOURNAL PLUS

Regular Article

Effect of frictional heating on radiative ferrofluid flow over a slendering stretching sheet with aligned magnetic field

J.V. Ramana Reddy[1], V. Sugunamma[1,a], and N. Sandeep[2,b]

[1] Department of Mathematics, S V University, Tirupati - 517502, India
[2] Department of Mathematics, VIT University, Vellore - 632014, India

Received: 7 November 2016 / Revised: 4 December 2016
Published online: 12 January 2017 –

Abstract. The pivotal objective of this paper is to look into the flow of ferrofluids past a variable thickness surface with velocity slip. Magnetite (Fe_3O_4) nanoparticles are embedded to the regular fluid. The occurrence of frictional heating in the flow is also taken into account. So the flow equations will be coupled and nonlinear. These are remodelled into dimensionless form with the support of suitable transmutations. The solution of the transformed equations is determined with the support of an effective Runge-Kutta (RK)-based shooting technique. Ultimately, the effects of a few flow modulating quantities on fluid motion and heat transport were explored through plots which are procured using the MATLAB tool box. Owing to the engineering applications, we also calculated the friction factor and the heat transfer coefficient for the influencing parameters. The results are presented comparatively for both regular fluid (water) and water-based ferrofluid. This study enables us to deduce that inflation in the aligned angle or surface thickness reduces the fluid velocity. The radiation and dissipation parameters are capable of providing heat energy to the flow.

Nomenclature

A, p, D	Constants
a	Maxwell's constant
$B(x)$	Applied magnetic field
B_M	Strength of the magnetic field
b	Thermal accommodation coefficient
C_f	Skin friction coefficient
Ec	Eckert number
g_1	Dimension free velocity slip parameter
g_2	Dimension free temperature jump parameter
k	Thermal conductivity
M	Magnetic field parameter
q_1	Dimensional quantity of velocity slip
q_2	dimensional quantity of temperature jump
R	Radiation parameter
T	Fluid temperature
Nu_x	Nusselt number (heat transfer rate)
T_w	Temperature near the surface
T_∞	Temperature faraway from the surface
Re_x	Reynolds number
u, v	Velocities along the x-, y-direction
u_w	Surface stretching velocity
m	Velocity power index

Greek symbols

μ	Dynamic viscosity
α	Aligned angle of the applied magnetic field
β_R	Mean absorption coefficient
δ	Volume fraction of solid nanoparticles
γ	Specific heats ratio
λ	Wall thickness parameter
ρ	Density
ρc_p	Heat capacitance of the fluid
σ	Electrical conductivity
σ_e	Stefan-Boltzmann constant
ζ_1, ζ_2	Mean free path constants
ξ, η	Similarity variables

Suffixes

ff	Ferrofluid
f	Base fluid
s	Solid particles

[a] e-mail: vsuguna@svuniversity.ac.in
[b] e-mail: dr.nsrh@gmail.com

1 Introduction

Normally, the regular fluids, namely water and oils, possess a restricted thermal conductivity, which makes them unacceptable for heavy refrigerating technologies. With the goal of intensifying that capability for regular fluids, solid nanoparticles, having high thermal conductivity, are integrated in them. This process results in a nanofluid. However, the inclusion of nanoparticles having magnetic behavior (for example; Fe_3O_4-H_2O) causes excessive thermal conductivity compared with ordinary nanofluids (for example, Cu-H_2O). Ferrofluids are nothing but magnetic nanofluids. The objective behind the invention of these fluids is to manage the heat transport in the flow field effectively. There are many important applications of ferrofluids in aerospace, medical, science and engineering. They are also used extensively in computer hard drives, to improve the function of loud speakers, etc., so, numerous authors have concentrated their research on the area of ferrofluid flows towards different geometries. The heat transport attributes of the fluid motion owing to the stretching of a surface have multitudinous benefits in chemical engineering operations. Viscous dissipation is capable of altering the temperature gradients by acting as energy source caused by frictional heating.

Anwar *et al.* [1] have addressed the radiation effects at the stagnation point flow along a stretching sheet. From their paper we may observes that the thermophoresis parameter makes the fluid temperature increase. The influence of frictional heat on the nanofluid through a stretching surface with a rotating frame was described by Wahiduzzaman *et al.* [2]. In this paper the authors used the visual `Fortran` software to obtain the results. Sugunamma *et al.* [3] addressed the fluid (comprising of solid nanoparticles) motion past a rotating frame. The domination of the Eckert number on the Casson fluid along a cylinder by taking the slip velocity was analysed by Makanda *et al.* [4] who found that enhancing the values of the Casson parameter results in the reduction of the fluid temperature. Biliana *et al.* [5] utilized the Keller-box numerical procedure for describing the flow across a surface, which stretches exponentially.

The study of magnetohydrodynamics has tremendous applications in the areas of cancer research, astrophysics, sensors, magnetic drug targeting and geophysics. The impact of rotation and radiation in the MHD flow through a flat surface was examined by Ramana Reddy *et al.* [6]. Anjali Devi and Prakash [7] presented a strange mathematical model to go through the impacts of varying viscosity, radiation on the MHD flow along a variable thickness stretching surface. It can be perceived from this paper that a rise in the magnitude of the velocity index parameter enhances the fluid temperature.

The study of the flows past a stretching surface with heat transfer plays an indispensable role in industrial processes like paper production, polymer extrusion, drawing of copper wires, metal extrusion, etc. Some papers [8–10] are concerned with the study of nanofluid flows across a stretching surface with suction/injection. Qasim *et al.* [11] explored the effects of velocity slip and heat transport on magnetohydrodynamic ferrofluid flow with heat flux. Sandeep and Sulochana [12] worked on heat transport attributes of dusty nanofluid flow caused by a stretching sheet. Mahanta and Shaw [13] addressed the MHD three-dimensional Casson fluid flows towards a melting surface. Akbar *et al.* [14] reported the flow characteristics of an Eyring-Powell fluid along a stretching surface with Lorentz force. Abel and Mahesha [15] explored the heat transfer attributes of viscoelastic liquid with varying thermal properties. Nadeem *et al.* [16] used the HAM to describe the flow of a Williamson fluid across a stretching surface. The motion of a ferrofluid caused by a gravity-aligned elastic sheet was studied by Titus and Abraham [17]. Das and Jana [18] explored the heat transport attributes of a magnetic nanofluid by employing the Laplace transformation technique. The influence of frictional heating on nanofluids along a heated surface was illustrated by Hussain *et al.* [19]. Babu *et al.* [20] worked on magnetic nanofluids to address the impact of nonlinear radiation. In this paper, they concluded that non-uniform heat has the propensity to regulate the fluid temperature. Aziz [21] examined the time-dependent flow due to vertical sheet considering variable viscosity. The impacts of radiation and Lorentz force on ferrofluid flows through a flat sheet with heat generation were investigated by Raju *et al.* [22] who concluded that heat transfer rate in a Fe_3O_4-kerosene ferrofluid is more than that of a Fe_3O_4-water ferrofluid. Ali and Sandeep [23] studied the heat transfer effects on MHD ferrofluid flow using the Cattaneo-Chrostov heat flux model and found that an increase in the volume fraction of ferroparticles causes a hike in the fluid velocity. Kennie *et al.* [24] discussed the flow of a viscous fluid over a nonlinear stretching curved surface and deduced that velocity and skin friction enhances effectively even for small variation in the curvature of stretching sheet. The impact of cross-diffusion on non-Newtonian nanofluid flows past a linearly stretched surface was examined by Ramzan *et al.* [25]. Khan and Azam [26] analyzed the heat transfer behaviour on the boundary layer flow of Carreau fluid along a stretching sheet.

Still, no effort has been made by the past researchers to go through the influences of frictional heat (viscous dissipation) and velocity slip on ferrofluid flows past a slendering stretching sheet. So, by taking the initiation, we make an attempt to fulfil this gap by exploiting the above-cited articles. Here the flow equations are remodelled into dimensionless form with the support of suitable transmutations. The solution of the transformed equations is determined with the support of an effective RK-based shooting technique.

2 Mathematical modelling of the problem

Let us consider a time-independent, 2D and electrically conducting motion of a ferrofluid across a thickness changeable sheet in the slip flow regime. The sheet is taken parallel to the x-axis and the y-axis is orthogonal to the sheet as

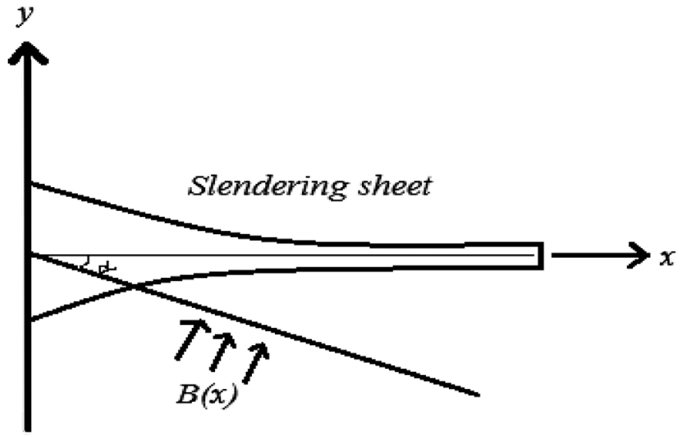

Fig. 1. Geometrical idea of the flow.

delineated in fig. 1. The aligned magnetic field $B(x) = B_0(x+p)^{0.5(1-m)}$ is exerted perpendicular to the sheet with an angle α.

The following suppositions have been built on the flow:

- The surface is assumed to stretch with velocity $u_w = A(x+p)^m$ and it is not permeable with $v_w = 0$.
- The flow surface is not flat and is described as $y = D(x+p)^{0.5(1-m)}$. Here D is small to describe the flow along the thinner sheet.
- Current problem exists only if $m \neq 1$, as $m = 1$ concerns the flow due to a flat stretched surface.

With respect to the aforestated presumptions, the constitutive equations determining the flow in the presence of radiation and frictional heating are given by (see Wahiduzzaman *et al.* [2] and Anjali Devi and Prakash [7])

$$\frac{\partial u}{\partial x} + \frac{\partial v}{\partial y} = 0, \tag{1}$$

$$\rho_{ff}\left(u\frac{\partial u}{\partial x} + v\frac{\partial v}{\partial y}\right) = \mu_{ff}\frac{\partial^2 u}{\partial y^2} - \sigma_{ff}B(x)^2\sin^2\alpha, \tag{2}$$

$$(\rho c_p)_{ff}\left(u\frac{\partial T}{\partial x} + v\frac{\partial T}{\partial y}\right) = k_{ff}\frac{\partial^2 T}{\partial y^2} + \mu_{ff}\left(\frac{\partial u}{\partial y}\right)^2 - \frac{\partial q_r}{\partial y}. \tag{3}$$

The boundary conditions with velocity slip are

$$\left.\begin{aligned} &u\left(x, D(x+p)^{0.5(1-m)}\right) = u_w + q_1\left(\frac{\partial u}{\partial y}\right), \\ &v\left(x, D(x+p)^{0.5(1-m)}\right) = 0, \\ &T\left(x, D(x+p)^{0.5(1-m)}\right) = T_w(x) + q_2\left(\frac{\partial T}{\partial y}\right), \\ &u(x,\infty) = 0, \quad T(x,\infty) = 0. \end{aligned}\right\} \tag{4}$$

In the above equation,

$$\begin{aligned} q_1 &= \left(\frac{2}{a} - 1\right)\zeta_1(x+p)^{0.5(1-m)}, \\ q_2 &= \zeta_2\left(\frac{2}{b} - 1\right)(x+p)^{0.5(1-m)}, \\ \zeta_2 &= \left(\frac{2\gamma}{\gamma+1}\right)\frac{\zeta_1}{\mathrm{Pr}}. \end{aligned}$$

In eqs. (1)–(3), u, v indicate the velocity components along the x-, y-direction, σ_{ff} is the electrical conductivity of the ferrofluid, T, T_w, respectively, denote temperature of the fluid and temperature along the sheet, T_∞ is the

temperature of the fluid in the free stream, ρ_{ff} is the ferrofluid density, μ_{ff} is the ferrofluid viscosity, $(\rho c_p)_{ff}$ is the ferrofluid heat capacitance and k_{ff} denotes the thermal conductivity of the ferrofluid. These are given as (see Ramana Reddy *et al.* [6])

$$\left.\begin{aligned}
&\rho_{ff} = (1-\delta)\rho_f + \delta\rho_s, \qquad \mu_{ff} = \frac{\mu_f}{(1-\delta)^{2.5}},\\
&(\rho c_p)_{ff} = (1-\delta)(\rho c_p)_f + \delta(\rho c_p)_s,\\
&\frac{\sigma_{ff}}{\sigma_f} = 1 + \frac{3(\sigma-1)\delta}{(\sigma+2)-(\sigma-1)\delta}, \quad \sigma = \sigma_s/\sigma_f\\
&\frac{k_{ff}}{k_f} = \frac{(k_s+2k_f)-2\delta(k_f-k_s)}{(k_s+2k_f)+\delta(k_f-k_s)}.
\end{aligned}\right\} \tag{5}$$

In view of the current investigation, the magnetic field and the wall temperature hold the following special forms:

$$B(x) = B_M(x+p)^{0.5(1-m)}, \qquad T_w(x) = T_\infty + T_0(x+p)^{0.5(1-m)}. \tag{6}$$

The radiative heat flux adheres to the Roseland approximation $q_r = \frac{-4\sigma_e}{3\beta_R}\frac{\partial T^4}{\partial y}$, where σ_e and β_R, respectively, signify the Stefan-Boltzmann, and the mean absorption constants. T^4 can be expressed as a Taylor series in terms of T_∞, then we get $T^4 \cong 4T_\infty^3 T - 3T_\infty^4$ (when higher-order terms are omitted).

We invoke the following similarity transmutations for changing the flow governing equations as a group of nonlinear ODEs:

$$\left.\begin{aligned}
&u = A(x+p)^m f'\\
&v = -\left(\xi f'\left(\frac{m-1}{m+1}\right) + f\right)\sqrt{0.5(m+1)\upsilon A(x+p)^{m-1}}\\
&\xi = y\sqrt{0.5(m+1)A\upsilon^{-1}(x+b)^{m-1}}\\
&T = T_\infty + \theta T_0(x+p)^{0.5(1-m)}.
\end{aligned}\right\} \tag{7}$$

With the help of eqs. (5)–(7), the momentum and energy equations arrive at

$$\begin{aligned}
&(1-\delta)^{-2.5}f''' - \left(1-\delta+\delta\left(\frac{\rho_s}{\rho_f}\right)\right)\left(2m(1+m)^{-1}f'^2 - ff''\right)\\
&-2(1+m)^{-1}\left(1+\frac{3(\sigma-1)\delta}{(\sigma+2)-(\sigma-1)\delta}\right)M\sin^2\alpha f' = 0,
\end{aligned} \tag{8}$$

$$\begin{aligned}
&\left(\frac{k_{ff}}{k_f}+R\right)\theta'' - \mathrm{Pr}\left(1-\delta+\delta\frac{(\rho C_p)_s}{(\rho C_p)_f}\right)\left((1-m)(1+m)^{-1}f'\theta - f\theta'\right)\\
&+(1-\delta)^{-2.5}Ec\,(f'')^2 = 0,
\end{aligned} \tag{9}$$

with dimensionless boundary restrictions

$$\left.\begin{aligned}
&f(\lambda) = \lambda\left(\frac{1-m}{1+m}\right)(1+g_1 f''(0)),\\
&f'(\lambda) = 1 + g_1 f''(0),\\
&\theta(\lambda) = 1 + g_2\theta'(0),\\
&f'(\infty) = \theta(\infty) = 0.
\end{aligned}\right\} \tag{10}$$

Here, in eq. (9), $M = \frac{\sigma B_0^2}{\rho U_0}$, $\mathrm{Pr} = \frac{\mu_f C_p}{k_f}$, $R = \frac{16\sigma_e T_\infty^3}{k_f\beta_R}$ and $Ec = \frac{U_w^2}{(c_p)_f T_0}$ are magnetic field parameter, Prandtl number, radiation parameter and Eckert number, respectively.

Also, in eq. (10),

$$\begin{aligned}
\lambda &= D\sqrt{0.5(1+m)\upsilon^{-1}A},\\
g_1 &= \left(\frac{2}{a}-1\right)\sqrt{0.5(1+m)\upsilon^{-1}A}\zeta_1,\\
g_2 &= \left(\frac{2}{b}-1\right)\sqrt{0.5(1+m)\upsilon^{-1}A}\zeta_2.
\end{aligned}$$

Table 1. Thermal and physical properties of H_2O and Fe_3O_4 solid particles. (See Babu *et al.* [20].)

Thermo-physical properties	Regular fluid (H_2O)	Fe_3O_4
ρ (Kg/m^3)	997.1	5180
c_p (J/Kg K)	4179	670
k (W/m K)	0.613	9.7
σ (S/m)	5.5×10^{-6}	0.74×10^6

Equations (8) and (9), along with the boundary restrictions given in eq. (10), are not linear ordinary differential equations having domain $[\lambda, \infty)$. So, for the calculation of the results in a simple way, it is better to change the domain to $[0, \infty)$. For that, we define a transformation F as $F(\eta) = F(\xi - \lambda) = f(\xi)$.

With respect to the new transformation defined above, eqs. (8)–(10) become

$$(1-\delta)^{-5/2}F''' - \left(1-\delta+\delta\left(\frac{\rho_s}{\rho_f}\right)\right)\left(\left(\frac{2m}{1+m}\right)F'^2 - FF''\right) - \left(\frac{2}{1+m}\right)\left(1+\frac{3(\sigma-1)\delta}{(\sigma+2)-(\sigma-1)\delta}\right)M\sin^2\alpha F' = 0, \tag{11}$$

$$\left(\frac{k_{ff}}{k_f}+R\right)\Theta'' - \Pr\left(1-\delta+\delta\frac{(\rho C_p)_s}{(\rho C_p)_f}\right)\left(\left(\frac{1-m}{1+m}\right)F'\Theta - F\Theta'\right) + (1-\delta)^{-5/2}Ec\,(F'')^2 = 0, \tag{12}$$

with the new boundary restrictions,

$$\left.\begin{aligned} &F(\lambda) = \lambda\left(\frac{1-m}{1+m}\right)(1+g_1F''(0)), \qquad F'(\lambda) = 1+g_1F''(0), \qquad \Theta(\lambda) = 1+g_2\Theta'(0), \\ &F'(\infty) = \Theta(\infty) = 0. \end{aligned}\right\} \tag{13}$$

We have also derived the expressions for friction factor and heat transfer coefficient due to their significance in engineering applications.

The skin-friction coefficient (C_f) is defined as (see Anjali Devi and Prakash [7])

$$C_f\,(\mathrm{Re}_x)^{\frac{1}{2}} = (1-\delta)^{-2.5}\sqrt{2(1+m)}F''(0). \tag{14}$$

Also, the Nusselt number is given by

$$Nu_x\,(\mathrm{Re}_x)^{\frac{-1}{2}} = -\left(\frac{k_{nf}}{k_f}+R\right)\sqrt{0.5(1+m)}\Theta'(0), \tag{15}$$

where $\mathrm{Re}_x = \frac{A(x+p)^{m+1}}{\upsilon_f}$ is the Reynolds number.

3 Analysis of the results

The group of altered ODE (11) and (12) according to the surface restrictions (13) has been solved with the aid of the Runge-Kutta shooting procedure. For results, we used the values of flow parameters as $\delta = 0.15$, $m = 3$, $M = 0.5$, $\alpha = \pi/4$, $\Pr = 7$, $R = 1.5$, $Ec = 0.5$, $\lambda = 0.2$ and $g_1 = g_2 = 0.3$. These values are fixed for the whole study, except for a distinction in the values as depicted in figures and tables. Table 1 presents the thermo-physical properties of H_2O and Fe_3O_4 nanoparticles.

Figures 2–13 show the domination of sundry parameters on the flow field. Further, table 2 reflects the impacts of the same parameters on friction factor and heat transfer coefficient for both regular fluid ($\delta = 0$) and Fe_3O_4-H_2O ferrofluid ($\delta = 0.15$) cases.

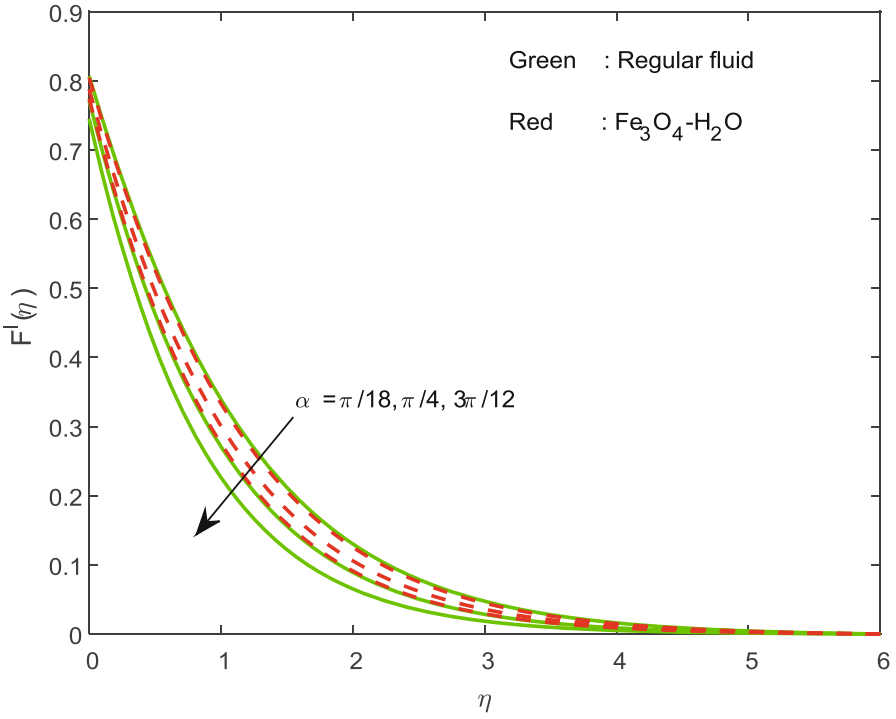

Fig. 2. Velocity profiles with varying aligned angle (α).

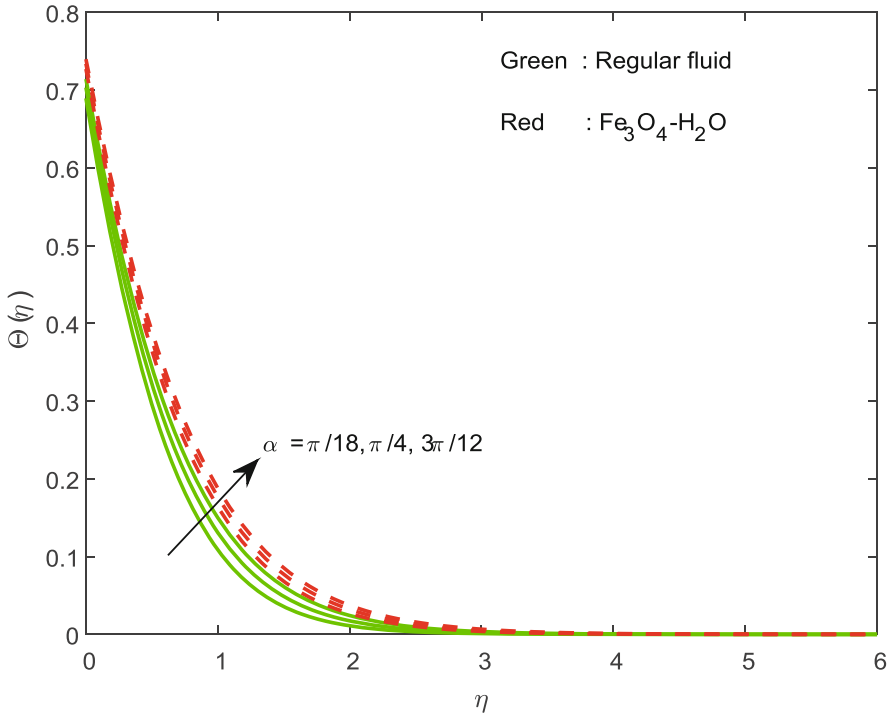

Fig. 3. Temperature profiles with varying aligned angle (α).

Figures 2 and 3 illustrate the nature of velocity and temperature fields with the effect of aligned angle (α). From fig. 2, it is easy to observe that greater values of the aligned angle reduces the fluid velocity. This may happen due to the Lorentz force, which works in the reversal way of the fluid motion. From fig. 3 we may observe that a rise in the aligned angle generates a hike in the temperature profiles. The cause behind this is that the Lorentz force works as an agent to provide heat to the fluid.

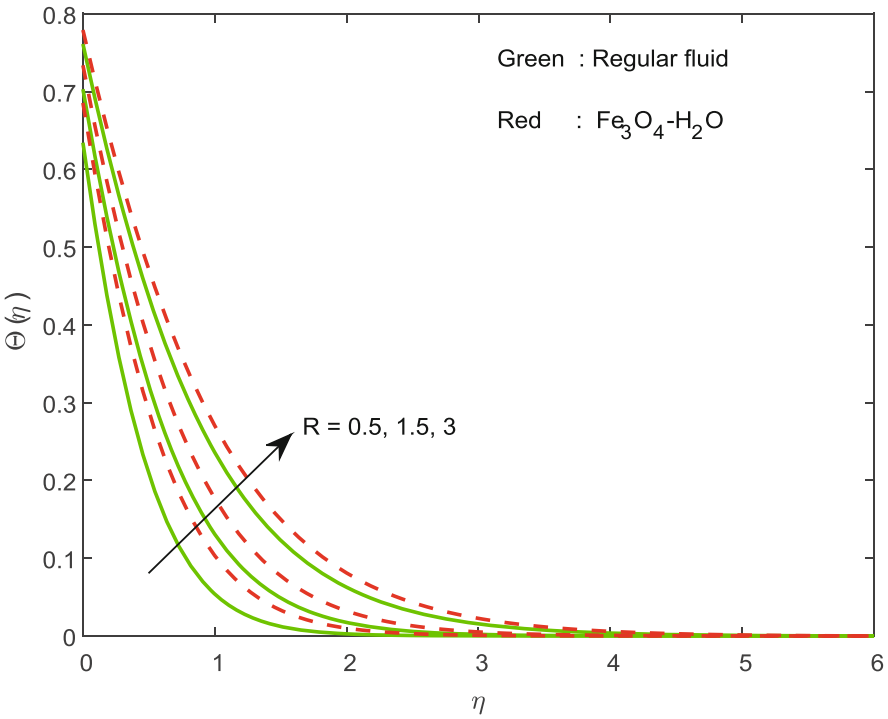

Fig. 4. Temperature profiles with varying radiation parameter (R).

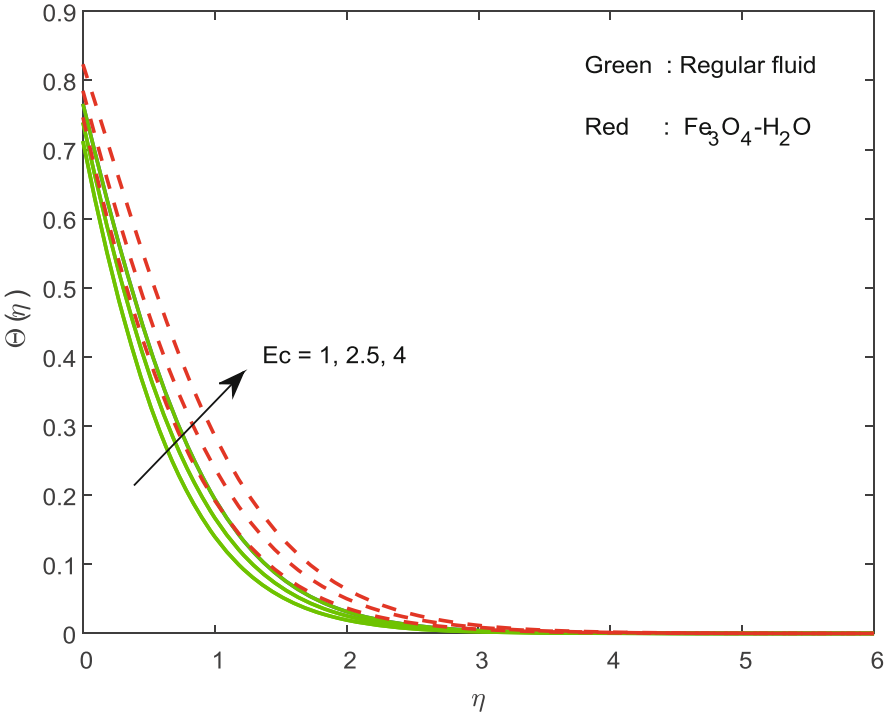

Fig. 5. Temperature profiles with varying Eckert number (Ec).

Figures 4, 5 and 6, respectively, show the influence of radiation parameter (R), Eckert number (Ec) and Prandtl number (Pr) on the temperature profiles. It is noteworthy, from figs. 4 and 5, that an increase in either radiation parameter or Eckert number causes an enhancement in the temperature profiles. But an opposite trend is noted under the impact of the Prandtl number, as depicted in fig. 6. Generally, a hike in radiation creates heat in the fluid and also an increase in the dissipation parameter helps the fluid move faster along the surface. These facts yield a thicker boundary layer.

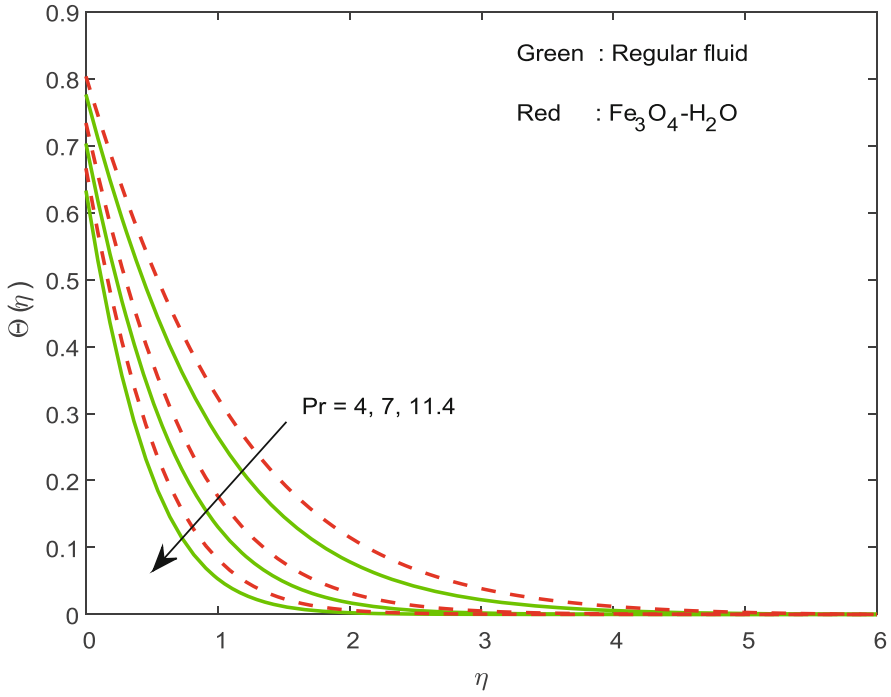

Fig. 6. Temperature profiles with varying Prandtl number (Pr).

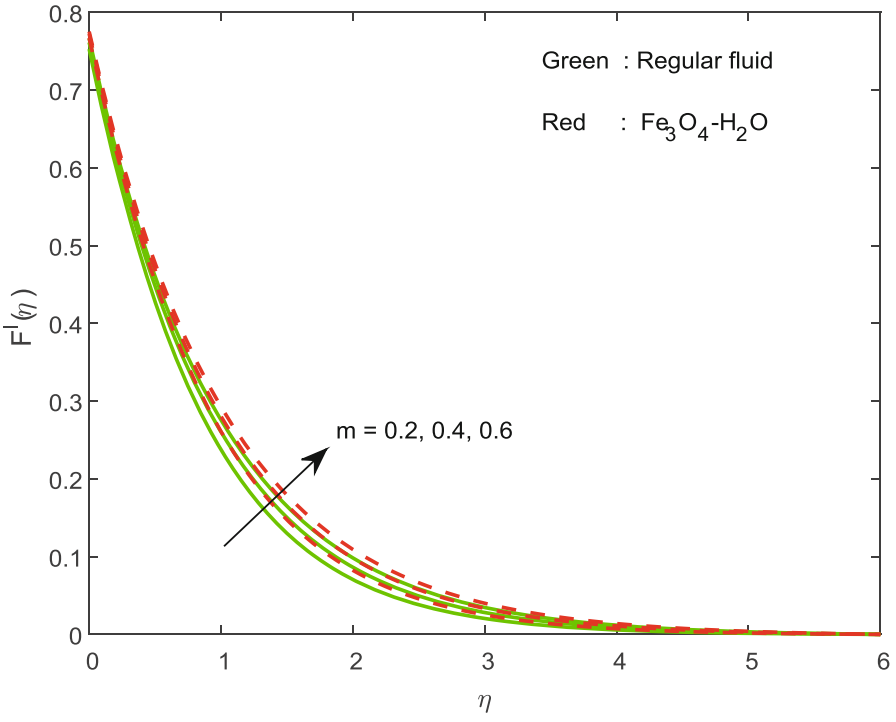

Fig. 7. Velocity profiles with varying velocity power index parameter (m).

Figures 7 and 8 are sketched to show the behaviour of the flow field with variation in the values of velocity power index parameter (m). It is clear, from fig. 7, that a growth in the magnitude of the velocity power index parameter induces intensification in the fluid velocity. Temperature distribution also rises with a hike in velocity power index parameter, as shown in fig. 8. This is because an increase in the velocity power index parameter cooperates to enrich the thermal boundary layer thickness.

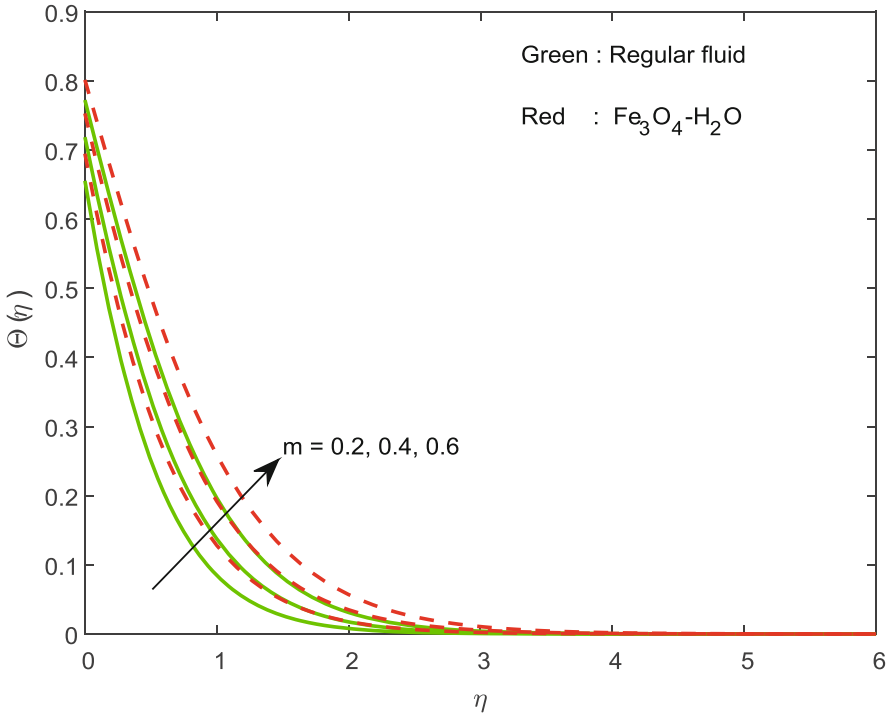

Fig. 8. Temperature profiles with varying velocity power index parameter (m).

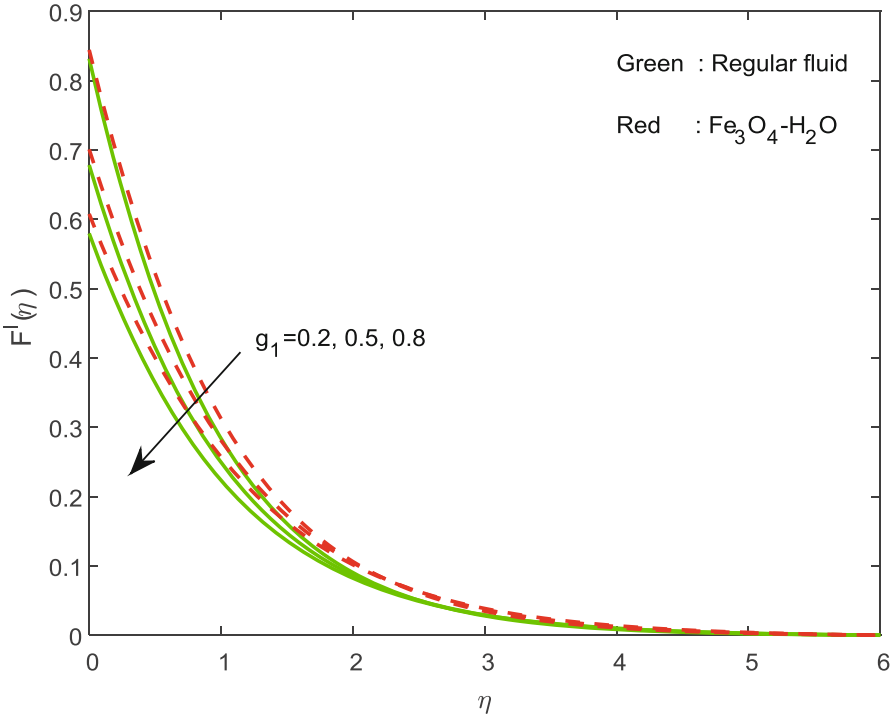

Fig. 9. Velocity profiles with varying velocity slip parameter (g_1).

Figure 9 shows the influence of the dimensionless slip velocity (g_1) on the velocity distribution. It is clear that an increase in the velocity slip parameter reduces the fluid motion. Actually, entire pulling force of the surface cannot be transfigured to the fluid, but it increases away from the sheet. Hence the slip velocity exerts a progressively diminishing effect leading to the reversed effect. Further, fig. 10 shows the effect of the velocity slip on the temperature profiles. This plot allows us to conclude that growing values of the velocity slip quantity increases the temperature profiles. This happens because the velocity slip parameter has propensity to increase the friction (heat source) in the flow.

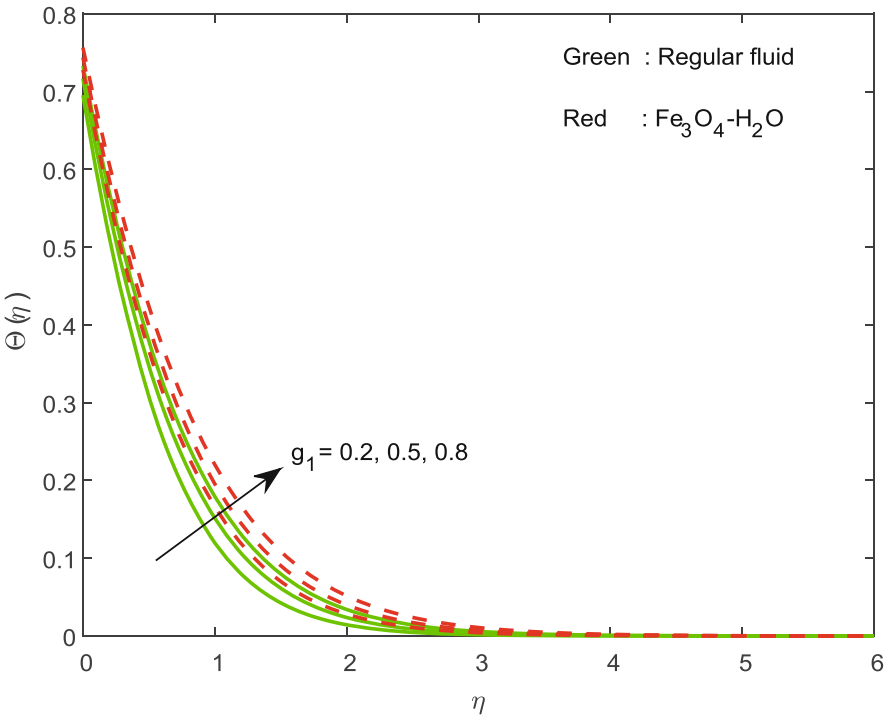

Fig. 10. Temperature profiles with varying velocity slip parameter (g_1).

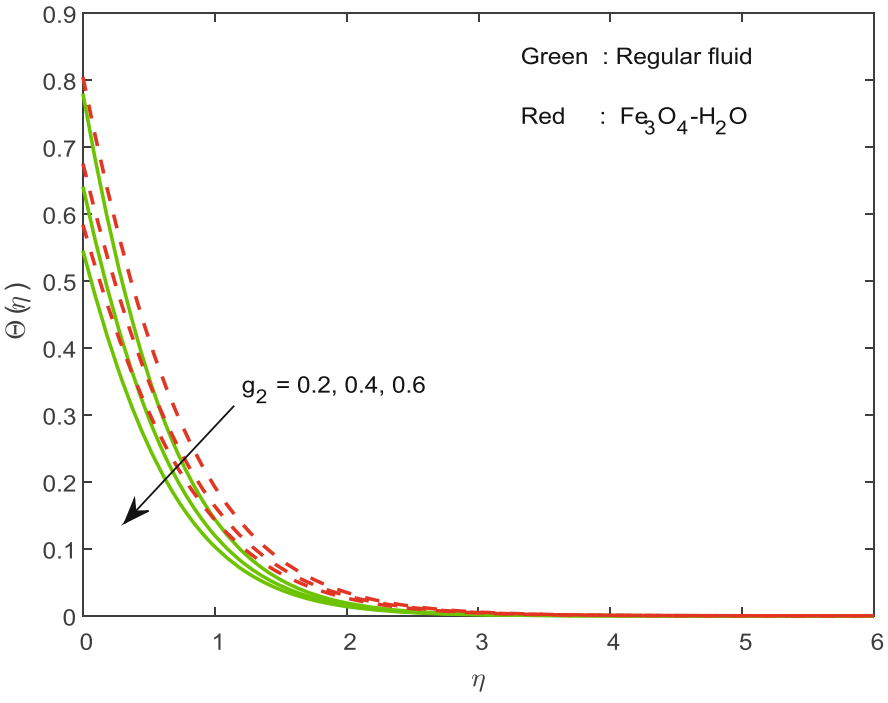

Fig. 11. Temperature profiles with varying temperature jump parameter (g_2).

Figure 11 shows the effect of the temperature jump parameter (g_2) on the fluid temperature. It is found that growing values of the temperature jump parameter reduce the temperature distribution in the flow. The reason behind this is that an increase in g_2 increases the thermal accommodation coefficient. Figures 12 and 13 depict the velocity and temperature behaviour under the action of the wall thickness parameter (λ). It is found that the wall thickness parameter is capable of controlling the velocity and temperature fields.

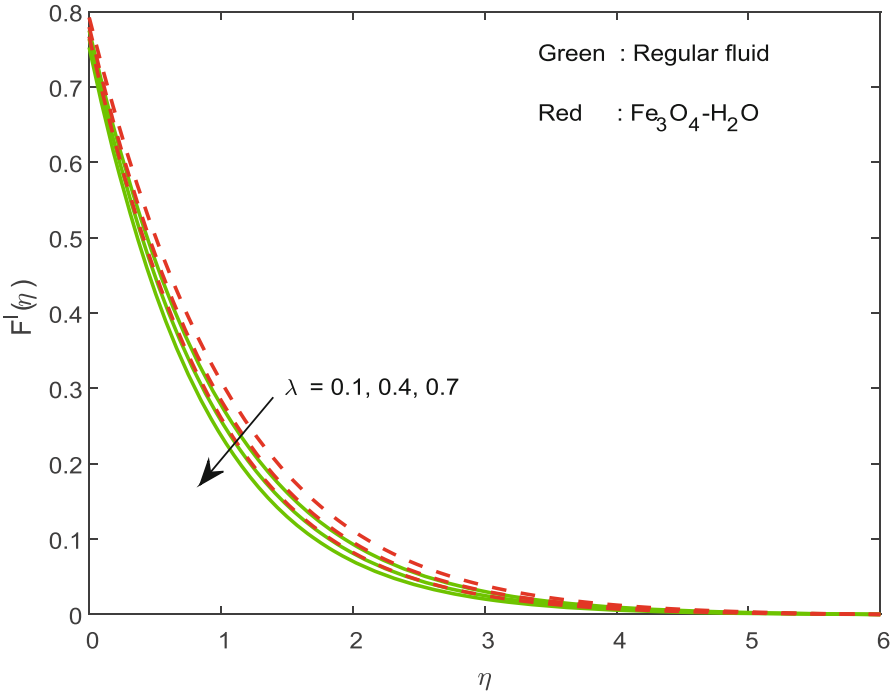

Fig. 12. Velocity profiles with varying wall thickness parameter (λ).

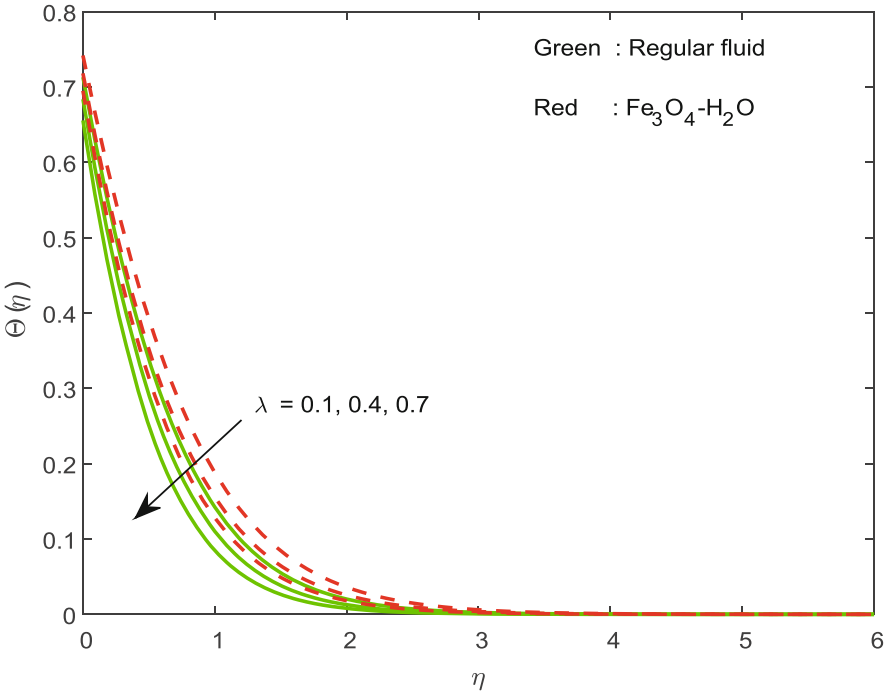

Fig. 13. Temperature profiles with varying wall thickness parameter (λ).

The fluctuations in the skin friction and Nusselt number with distinct flow parameters are presented in table 2. This table enables one to see that an increase in the aligned angle (α) and wall thickness parameter (λ) helps minimize the friction at the surface, while the friction near the surface becomes strong with a hike in the velocity power index parameter (m) or velocity slip parameter (g_1). Further, we observe a gradual reduction in the Nusselt number with larger values of aligned angle (α), radiation parameter (R), Eckert number (Ec), velocity power index parameter (m), velocity slip parameter (g_1) and temperature jump parameter (g_2). But the Prandtl number (Pr) or the wall thickness parameter (λ) enhance the heat transfer rate effectively. From table 3, we can see a favourable agreement of the present results with published work [27].

Table 2. Variations of skin friction and Nusselt number for regular fluid ($\delta = 0$) and Fe_3O_4-H_2O ($\delta = 0.15$).

α	R	Ec	Pr	m	g_1	g_2	λ	Friction factor		Nusselt number	
								$\phi = 0$	$\phi = 0.15$	$\phi = 0$	$\phi = 0.15$
$\pi/18$								−0.6428	−0.6505	1.0354	0.9098
$\pi/4$								−0.7619	−0.7061	0.9894	0.8871
$5\pi/12$								−0.8488	−0.7519	0.9530	0.8677
	0.5							−0.7619	−0.7061	1.1218	1.0483
	1.5							−0.7619	−0.7061	0.9894	0.8871
	3							−0.7619	−0.7061	0.7955	0.7358
		1						−0.7619	−0.7061	0.9593	0.8445
		2.5						−0.7619	−0.7061	0.8691	0.7165
		4						−0.7619	−0.7061	0.7790	0.5886
			4					−0.7619	−0.7061	0.7452	0.6550
			7					−0.7619	−0.7061	0.9894	0.8871
			11.4					−0.7619	−0.7061	1.2236	1.1128
				0.2				−0.8244	−0.7766	1.1479	1.0170
				0.4				−0.7960	−0.7590	0.9374	0.8230
				0.6				−0.7788	−0.7496	0.7585	0.6613
					0.2			−0.8417	−0.7787	1.0153	0.9061
					0.5			−0.6436	−0.5983	0.9443	0.8535
					0.8			−0.5255	−0.4903	0.8890	0.8113
						0.2		−0.7619	−0.7061	1.1017	0.9781
						0.4		−0.7619	−0.7061	0.8978	0.8117
						0.6		−0.7619	−0.7061	0.7576	0.6936
							0.1	−0.7493	−0.6920	0.9566	0.8607
							0.4	−0.7869	−0.7344	1.0540	0.9397
							0.7	0.8244	−0.7766	1.1479	1.0170

Table 3. Comparison of the present results for $f''(0)$ with those of [27] when $R = M = g_2 = \phi = 0$, $m = 0.5$.

λ	g_1	Khader and Megahed [27]	Present study
0.2	0	−0.924828	−0.92482810
0.25	0.2	−0.733395	−0.73339523
0.5	0.2	−0.759570	−0.75957013

4 Concluding remarks

The effects of assorted physical parameters on the movement of ferrofluids across a surface of variable thickness are explored. The equations which explain the flow situation are altered into dimensionless ODE, exploiting the similarity transforms. Afterwards, the problem's solution is obtained exploiting the RK shooting method. Finally, we studied the effects of flow-regulating parameters via plots and a table and conclude with the following observations:

- An increase in the values of the aligned angle (α) or velocity slip parameter (g_1) reduces the velocity of the fluid but increases the temperature.
- A growth in either radiation parameter (R) or Eckert number (Ec) enhances the fluid temperature.
- An enhancement in the velocity as well as in the temperature profile in observed for increasing values of the velocity power index parameter (m).
- Increasing values of the aligned angle (α) or wall thickness parameter (λ) reduces the friction factor, whereas the friction factor increases with the velocity power index parameter (m).
- An increase in any of the parameters, such as aligned angle (α), radiation parameter (R), Eckert number (Ec), velocity power index parameter (λ), velocity slip parameter (g_1), temperature jump parameter and (g_2) can reduce the Nusselt number.

References

1. M.I. Anwar, S. Sharidan, I. Khan, M.A. Salleh, Indian J. Chem. Tech. **21**, 199 (2014).
2. M. Wahiduzzaman, M.S. Khan, P. Biswas, I. Karim, M.S. Uddin, Appl. Math. **6**, 547 (2015).
3. V. Sugunamma, J.V. Ramana Reddy, C.S.K. Raju, M. Jayachandrababu, N. Sandeep, Indust. Eng. Lett. **4**, 8 (2014).
4. G. Makanda, S. Shaw, P. Sibanda, Bound. Value Probl. **2015**, 75 (2015).
5. B. Biliana, N. Roslinda, Eur. J. Sci. Res. **33**, 710 (2009).
6. J.V. Ramana Reddy, V. Sugunamma, N. Sandeep, C. Sulochana, J. Niger. Math. Soc. **35**, 48 (2016).
7. S.P. Anjalidevi, M. Prakash, J. Niger. Math. Soc. **34**, 318 (2015).
8. K. Bhattacharyya, G.C. Layek, Phys. Res. Int. **2014**, 512536 (2014).
9. S. Mukhopadhyay, Ain Shams Eng. J. **4**, 485 (2013).
10. J.V. Ramana Reddy, V. Sugunamma, N. Sandeep, P. Mohankrishna, Adv. Sci. Eng. Med. **7**, 753 (2015).
11. M. Qasim, Z.H. Khan, W.A. Khan, I.A. Shah, PLoS ONE **9**, e83930 (2014).
12. N. Sandeep, C. Sulochana, Ain Shams Eng. J. **7**, 709 (2016).
13. G. Mahanta, S. Shaw, Alex. Eng. J. **54**, 653 (2015).
14. N.S. Akbar, A. Ebaid, Z.H. Khan, J. Magn. & Magn. Mater. **382**, 355 (2015).
15. M.S. Abel, N. Mahesha, Appl. Math. Model. **32**, 1965 (2008).
16. S. Nadeem, S.T. Hussain, C. Lee, Brazil. J. Chem. Eng. **30**, 619 (2013).
17. L.S. Titus, A. Abraham, J. Appl. Fluid Mech. **8**, 591 (2015).
18. S. Das, R.N. Jana, Alex. Eng. J. **54**, 55 (2015).
19. T. Hussain, S.A. Shehzad, A. Alsaedi, T. Hayat, M. Ramzan, J. Cent. South Univ. **22**, 1132 (2015).
20. M.J. Babu, N. Sandeep, C.S.K. Raju, J.V.R. Reddy, V. Sugunamma, J. Adv. Phys. **5**, 302 (2016).
21. M.A.E. Aziz, J. Egypt. Math. Soc. **22**, 529 (2014).
22. C.S.K. Raju, N. Sandeep, C. Sulochana, V. Sugunamma, Int. J. Sci. Eng. **8**, 151 (2015).
23. M.E. Ali, N. Sandeep, Results Phys. **7**, 21 (2017).
24. S.M. Kennie, S. Asghar, M. Jalil, O.N. Fidelis, Results Phys. **7**, 1 (2017).
25. M. Ramzan, M. Bilal, J.D. Chung, U. Farooq, Results Phys. **6**, 1071 (2016).
26. M. Khan, M. Azam, Results Phys. **6**, 1168 (2016).
27. M. Khader, A.M. Megahed, Eur. Phys. J. Plus **128**, 100 (2013).